Breakdown and Limit of Continuum Diffusion Velocity for Binary Gas Mixtures from Direct Simulation

Robert Scott Martin and Farrokh Najmabadi

Center for Energy Research, University of California San Diego, 457 EBU-II, 9500 Gilman Drive, MC 0417, La Jolla, CA 92093-0417, USA

Abstract.
This work investigates the breakdown of the continuum relations for diffusion velocity in inert binary gas mixtures. Values of the relative diffusion velocities for components of a gas mixture may be calculated using of Chapman-Enskog theory and occur not only due to concentration gradients, but also pressure and temperature gradients in the flow as described by Hirschfelder. Because Chapman-Enskog theory employs a linear perturbation around equilibrium, it is expected to break down when the velocity distribution deviates significantly from equilibrium. This breakdown of the overall flow has long been an area of interest in rarefied gas dynamics. By comparing the continuum values to results from Bird's DS2V Monte Carlo code, we propose a new limit on the continuum approach specific to binary gases. To remove the confounding influence of an inconsistent molecular model, we also present the application of the variable hard sphere (VSS) model used in DS2V to the continuum diffusion velocity calculation. Fitting sample asymptotic curves to the breakdown, a limit, V_{max}, that is a fraction of an analytically derived limit resulting from the kinetic temperature of the mixture is proposed. With an expected deviation of only 2% between the physical values and continuum calculations within $\pm V_{max}/4$, we suggest this as a conservative estimate on the range of applicability for the continuum theory.

Keywords: Binary Mixture, Diffusion Velocity, Breakdown, Direct Simulation Monte Carlo
PACS: 51.20.+d

INTRODUCTION

The primary goal of this work is to determine the range of applicability for the continuum model for diffusion velocity. We plan to apply the resulting limit to diffusion velocities in continuum simulations of gas mixtures in future work. In hybrid codes such as those of Garcia and Bell in References [1, 2], criteria are also needed for predicting the breakdown of the continuum model for algorithm adaptation. We hope this limit serves as one such criteria for breakdown in diffusion velocity to ensure a consistent handoff between algorithms.

Our group investigates the response of low density gas within potential inertial fusion energy (IFE) power plant chamber designs between subsequent fusion events [3, 4]. We began studying the multi-component extensions to the Navier-Stokes equations because fusion byproducts will accumulate in the chamber during steady state operation. In extending our code to multi-component mixtures, we found that the strong pressure and temperature gradients drive the gas mixture composition out of equilibrium within the chamber due to the thermal- and baro-diffusive effects as predicted by Chapman-Enskog theory [5].

Sherman used Chapman-Enskog theory to analytically solve for the structure of shocks in binary gas mixtures [6]. When this solution was applied to mixtures with trace heavy component gas, it was shown to produce erroneous undershoots in the heavy component density both experimentally by Center [7] and numerically by Bird [8]. Since these early results, continuum solutions for gas mixtures generally neglect the thermal- and baro-diffusive effects in favor of Fickian diffusion only. Some early exceptions include the work at Sandia National Laboratories on transport properties for combustion [9] and the work on stability in Rayleigh Bénard flow for binary mixtures by Gutcowicz [10, 11] and Abernathey [12]. The Rayleigh Bénard work is interesting in that it demonstrates a significant destabilizing effect resulting from thermal diffusion without any rarification. This suggests that the effect may have significant macroscopic consequences in continuum flows and should not be neglected a priori. A thorough description of recent advances in multicomponent flow modeling is found in Giovangigli's work [13].

While validating our multi-component code, we found nearly identical results to Sherman's solution when applied to 1D-shock waves [5]. Though this result included the erroneous density undershoot, it provided confidence that the results were consistent with Chapman-Enskog theory and likely valid in regions of the flow close to equilibrium. It also sparked our interest in the nature of this type of breakdown in the continuum theory.

The case that produced the most significant undershoot in our validation studies was a He:Xe mixture shock at Mach 4.38 with 3% Xe based on Herczynski's experimental setup [14]. The shock produced diffusion velocities on the order of the sound speed in our calculations. In this earlier work [5], we considered applying a limit on the diffusion velocity with bounds at the thermal speed based on Oran's suggestion of a limit of a few percent of the thermal speed [15]. Applying this limit to the our validation cases, we found that it produced no change for the weak shocks but significantly narrower shocks with less undershoot for the strong shock case. With only a few experimental results available, we could not determine an optimal fraction of the thermal velocity for the diffusion velocity limit or even whether it should include a dependence on local composition.

In this work we attempt to answer these question using Bird's DS2V Monte Carlo code to perform computational experiments across a wide range of flow conditions. We use mixtures of noble gases in under-expanded jets based on Rothe's experimental setup [16, 17] to probe these conditions. The continuum diffusion velocities are calculated using the average pressure, density, composition and temperature fields from the DS2V solution to avoid confounding influences from other continuum breakdowns expected in a full continuum solution.

CALCULATION OF DIFFUSION VELOCITY

The diffusion velocity, V_{is}, is defined in Equation 1 as the difference between the average velocity of particles in one gas species relative to the mixture mass average velocity, v_{i0}, of the bulk fluid defined in Equation 2. Equation 3 shows the constitutive relation for the diffusion velocity of the s^{th} species in a mixture resulting from Chapman-Enskog theory. The formulation follows that of Reference [9] using a mixture diffusion coefficient, D_{sm}, defined in terms of the normal binary diffusion coefficients, $\mathscr{D}_{rs}$, in Equation 4. The binary diffusion coefficient is calculated in terms of the average molecular diameter, d_{rs}, reduced mass, m_{rs}, and collision integral, $\Omega_{rs}^{1,1\star}$ as shown in Equation 5. The thermal diffusion ration, Θ_s, to first approximation is shown in Equation 6 in terms of k_{rs} as seen in Equation 7. The ratios of collision integrals, $A^\star, B^\star$, and $C^\star$, are all equal to unity for the hard sphere model and are generally weak functions of temperature for other inter-molecular force models.

$$V_{is} \equiv \overline{v}_{is} - v_{i0} \tag{1}$$

$$\rho v_{i0} \equiv \frac{1}{\rho} \sum_{s=1}^{N_s} \rho_s \overline{v}_{is} \tag{2}$$

$$\vec{V}_s = -D_{sm} \left[\frac{\nabla X_s}{X_s} + \left(1 - \frac{m_s}{\overline{m}}\right) \frac{\nabla P}{P} + \frac{\Theta_s}{X_s} \frac{\nabla T}{T} \right] \tag{3}$$

$$D_{sm} = \frac{1 - Y_s}{\sum_{r \neq s} X_s \mathscr{D}_{rs}} \tag{4}$$

$$\mathscr{D}_{rs} = \frac{3}{16} \frac{(2\pi k T / m_{rs})^{1/2}}{n \pi d_{rs}^2 \Omega_{rs}^{1,1\star}} \tag{5}$$

$$\Theta_s = \sum_{r \neq s} k_{rs} X_r X_s \frac{m_s - m_r}{m_r + m_s} \tag{6}$$

$$k_{rs} = \frac{15}{2} \frac{(2A_{rs}^\star + 5)(6C_{rs}^\star - 5)}{A_{rs}^\star (16A_{rs}^\star - 12B_{rs}^\star + 55)} \tag{7}$$

To ensure the Monte Carlo and continuum diffusion velocities differences result from a breakdown in the continuum approach rather than the molecular model, collision integrals using the variable soft sphere (VSS) molecular model are needed. Equation 8 shows these integrals as derived from Bird's description of the VSS model using Chapman-Enskog theory [18]. In the collision integrals, $\nu + 1/2$ is the temperature viscosity power law, α is the VSS parameter adjusted to match both the viscosity and diffusion coefficient, and E_{ref} is a constant defined to match the gas viscosity at a reference temperature. For collisions between unlike species, the mixture values of these parameters were calculated using the averages found in source of Bird's DSMC0 code [18] to ensure an equivalent treatment with DS2V.

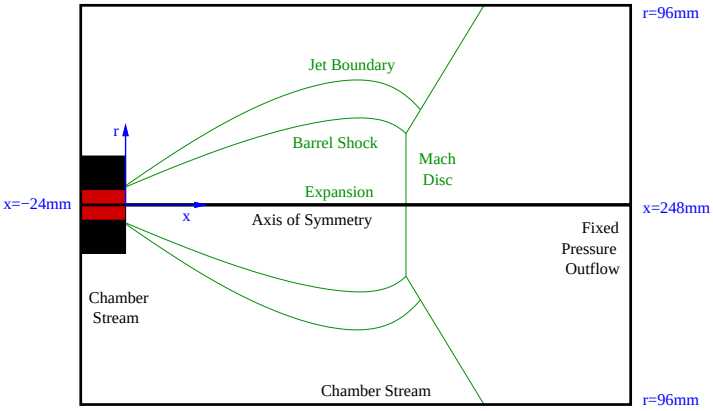

FIGURE 1. Monte Carlo geometry (blue) and boundary conditions (black) relative to flow regions (green). The inside of the nozzle is marked in red to denote fixed choked sonic conditions within the region.

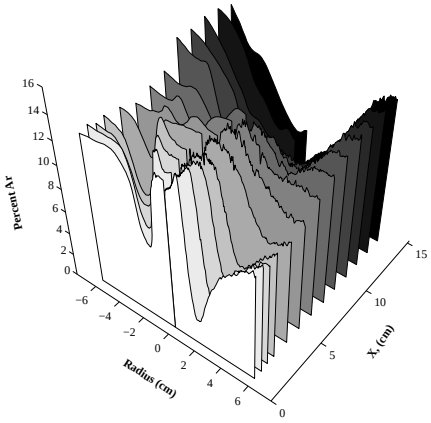

FIGURE 2. Argon molar percentage throughout the flow. Front side shows Monte Carlo solution and back side shows experimental results from Rothe's electron beam study.

$$
\begin{aligned}
\Omega_{VSS}^{1,1\ \star} &= \frac{\Gamma(3-\nu)}{2}\left(\frac{E_{ref}}{2kT}\right)^{\nu}\frac{2}{\alpha+1} \\
\Omega_{VSS}^{1,2\ \star} &= \frac{\Gamma(4-\nu)}{6}\left(\frac{E_{ref}}{2kT}\right)^{\nu}\frac{2}{\alpha+1} \\
\Omega_{VSS}^{1,3\ \star} &= \frac{\Gamma(5-\nu)}{24}\left(\frac{E_{ref}}{2kT}\right)^{\nu}\frac{2}{\alpha+1} \\
\Omega_{VSS}^{2,2\ \star} &= \frac{\Gamma(4-\nu)}{6}\left(\frac{E_{ref}}{2kT}\right)^{\nu}\frac{6\alpha}{(\alpha+1)(\alpha+2)}
\end{aligned}
\tag{8}
$$

COMPARISON OF CONCENTRATIONS AND DIFFUSION VELOCITIES FOR EXPERIMENTAL CONDITIONS

Rothe's experimental setup [16, 17] for electron beam studies of He:Ar mixture under-expanded free jets was used for boundary conditions in DS2V. In the experiment, a 12% argon mixture at 2.56 mmHg expands through a 15 mm diameter sonic orifice into a chamber at a pressure of 17 μmHg. This orifice was in a flat plate affixed to a 47.5 mm diameter converging nozzle. In the simulations, a uniform choked flow is used to approximate the plate orifice. Figure 1 shows the numerical domain used in DS2V as well as its reflection over the axis of symmetry. The flow from the nozzle is shown broken down into regions consisting of the expansion, Mach disc, barrel shock, and streamline jet boundary. Flow within the expansion closely resembles a 1D spherical expansion centered slightly downstream of the orifice. The diffusion velocities within this region remain relatively small, consistent with Bird's result for 1D free expansions [18]. However, in the Mach disc and barrel shock large diffusion velocities produce significant composition variation. Rothe's setup was selected because experimentally measured argon concentrations throughout the flow are provided. Figure 2 shows both the DS2V and experimental concentrations adjacent to each other. This figure shows that DS2V reproduces the concentration variations within the jet providing confidence in DS2V's diffusion velocities.

The only significant difference between the experiment and DS2V's results occur in the region outside the edge of the jet extending to the boundary. This difference is likely due to differential vacuum pumping fluxes between the gases [19] which would result in argon enrichment within the chamber in the experiment. Because this value was not experimentally measured beyond the apparent composition at the edge, in this work the chamber boundary conditions

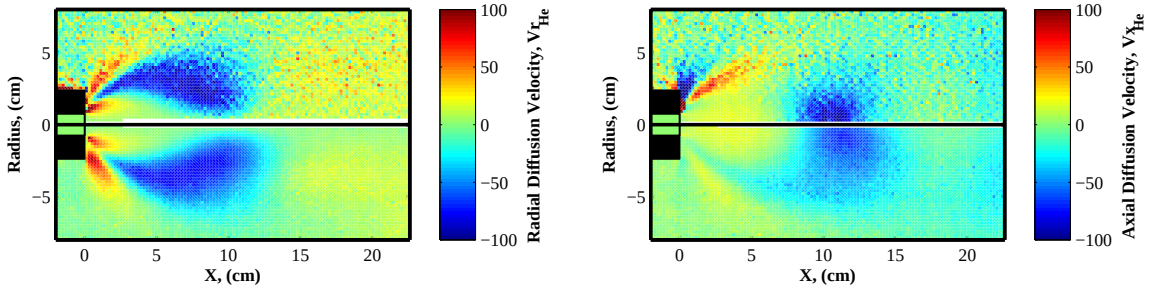

FIGURE 3. Comparison of radial (left) and axial (right) diffusion velocities in (m/s) between the DS2V results (bottom) and equivalent continuum values (top).

were set to equal the jet composition. Regardless of the true chamber composition, because the continuum diffusion velocity calculation depends only on the DS2V fields, the continuum calculation remains consistent with DS2V's results for the remainder of this work.

Figure 3 shows the radial and axial components of the diffusion velocity for the experimental configuration as calculated by DS2V as well as the associated velocities based on the continuum formulas resulting from DS2V's average pressure, density, and temperature fields. Note that the continuum results appear noisier than the Monte Carlo side because the derivatives of the average fields needed to calculate the diffusion velocity amplify the fluctuations inherent in the Monte Carlo result. Other than this noise, the largest discrepancy appears between the axial diffusion velocities in the highly rarefied region adjacent to the nozzle.

DIFFUSION VELOCITY LIMIT

The diffusion velocity and transport coefficients result from Chapman-Enskog theory and therefore assume a small perturbation from equilibrium for the velocity distribution. Within shocks and rarefied flows, both of these assumptions can break down. For mixtures, the perturbation assumption clearly fails whenever the diffusion velocities are large relative to the thermal velocity. The theory also assumes sufficient collisionality to ensure equal and isotropic temperatures for all gas components. To derive an absolute upper limit on the diffusion velocity for a given mixture kinetic temperature, we consider Bird's definitions of the kinetic temperature and species kinetic temperature [18] as seen in Equations 9 and 10. This species kinetic temperature can be shown to be proportional to the sum of squares about the species mean velocity plus the square of the species diffusion velocity. Equation 11 combines these equations defining an individual species thermal velocity $c_{i_s}^2 \equiv \overline{(v_{is} - \overline{v_{is}})^2}$ for the sake of readability.

$$\frac{3}{2} k T_{tr} = \frac{1}{2} \sum_{s=1}^{N_s} X_s m_s \overline{(v_{is} - v_{i0})^2} \tag{9}$$

$$\frac{3}{2} k T_{trs} = \frac{m_s}{2} \overline{(v_{is} - v_{i0})^2} = \frac{m_s}{2} \left(\overline{(v_{is} - \overline{v_{is}})^2} + V_{is}^2 \right) \tag{10}$$

$$3 k T_{tr} = \sum_{s=1}^{N_s} X_s m_s \left(c_{i_s}^2 + V_{is}^2 \right) \tag{11}$$

We define a Cartesian velocity coordinate system such that the diffusion velocity is aligned to the v_x-coordinate. The expansion of Equation 11 for these coordinates is shown in Equation 12. Consistent with the single isotropic temperature assumption of Chapman-Enskog theory, we assume the contributions of each direction's kinetic energy is equal to the overall kinetic temperature therefore the continuum temperature. Using this assumption, Equation 13 shows the remaining v_x direction contribution. This equation can then be simplified to relate the quantities back to the bulk sound speed, a, as seen in Equation 14.

$$T_{tr} = \frac{1}{3}\left(T_{trx} + T_{try} + T_{trz}\right) = \frac{1}{3k}\sum_{s=1}^{N_s} X_s m_s \left((c_{x_s}^2 + V_{x_s}^2) + c_{y_s}^2 + c_{z_s}^2\right) \tag{12}$$

$$T_{trx} = \frac{1}{k}\sum_{s=1}^{N_s} X_s m_s \left(c_{x_s}^2 + V_{x_s}^2\right) = T_{tr} \tag{13}$$

$$a^2/\gamma = \frac{kT_{tr}}{\overline{m}} = \sum_{s=1}^{N_s} Y_s \left(c_{x_s}^2 + V_{x_s}^2\right) \tag{14}$$

For binary mixtures, this can be taken further to provide a bound on the diffusion velocity. The maximum diffusion velocity occurs when $c_{i_s}^2 = 0$ for one of the gas species. This does not necessarily occur simultaneously for both gases, yet the limits are connected through the definition of the diffusion velocity. Combining the definitions of the diffusion velocity and mass average velocity, it can be shown that the species densities multiplied by diffusion velocities sum to zero as seen in Equation 15. This means that for a binary mixture, $\rho_1 V_{i1} = -\rho_2 V_{i2}$. Using this relationship, we define a mean diffusion velocity, $\hat{V}_i = \sqrt{\rho_1/\rho_2}V_{i1} = -\sqrt{\rho_2/\rho_1}V_{i2}$ such that both components of diffusion velocity can be scaled to be equal in magnitude in opposite directions. Next we assume that $(c_{x_r}^2 + V_{x_r}^2)$ is equal to the thermal velocity squared of the species, kT_{tr}/m_r, in the species that is not limited while $c_{x_s}^2 = 0$ in the limited direction. Using the $\hat{V}$ definition in Equation 14 results in Equation 16 after simple algebraic manipulation.

$$\sum_s \rho_s V_{is} = 0 \tag{15}$$

$$\left|\hat{V_x}^2\right|_{max} = \frac{a^2}{\gamma}\min\left(\frac{X_1}{Y_2}, \frac{X_2}{Y_1}\right) \tag{16}$$

We can now define the species maximum as $V_{max_s} = \frac{1}{2}\sqrt{\rho_r/\rho_s}\left|\hat{V}_x\right|_{max}$. Scaling both velocity components by their corresponding V_{max_s} allows the components to be plotted symmetrically together because $V_s/V_{max_s} = -V_r/V_{max_r}$. Figure 4(a), shows an example case for a He:Ar jet with a 50:50 composition. Figure 4(b-c) contains plots for He:Ar, He:Xe, and Ar:Xe systems. Each figure is the sum of 9 initial jet mixtures such as the one depicted in Figure 4(a). Each set of 9 ranges between 10:90 and 90:10 in 10% increments. The plots use a log scale with the color representing the number of points, N, contained by each cell on a grid with a resolution of 100-cells per 1 normalized velocity unit. In Figure 4, we scale both the Monte Carlo (DSMC) and continuum (Cont.) diffusion velocity calculations by these V_{max} limits.

A *tanh* curve is included based on a best fit for the data points across a wide range of gases and mixtures against several test curves including $tanh$, erf, and a scaled tan^{-1}. The test curves were selected with the constraints that the curve's slope must be 1:1 near the origin where the perturbations from equilibrium are small and that the curve must asymptote to ± 1 at infinity. The factor of $1/2$ in the limit resulted from this fitting procedure as well though cases with more significant breakdown are needed to confirm this result because the fitting procedure breaks down for cases when the points do not deviate significantly beyond the noise relative to the 1:1 line.

Though the bulk of the points lie on or near the 1:1 line near the origin, the plots all exhibit a bulge around the origin. This is due in large part to the noise in the low density region exterior to the jet. This can be seen in the noise on the top half of the plots in Figure 3. The flowfield output of DS2V lacks sampling cell grid information providing only unstructured point values. Significant noise is introduced from resampling these unstructured data points onto a uniform mesh to calculate the diffusion velocities. Coarse uniform meshes under-predict the maximum diffusion velocities because the gradients are reduced. Fine meshes capture the maximum velocities but produce noise because of erroneous gradient calculations from sub-sampling the coarse sampling cells in highly rarefied regions of the flow.

CONCLUDING REMARKS

The results would be improved if the continuum diffusion velocity calculation was internalized in the Monte Carlo solver and averaged over multiple steps rather than at one snapshot solution. This change would also enable calculation of continuum diffusion velocities on the natural DS2V sampling cell grid rather than an artificial uniform mesh. With these change, the fluctuations in the highly rarefied portion of the flow could be significantly reduced providing a clearer view of the continuum breakdown.

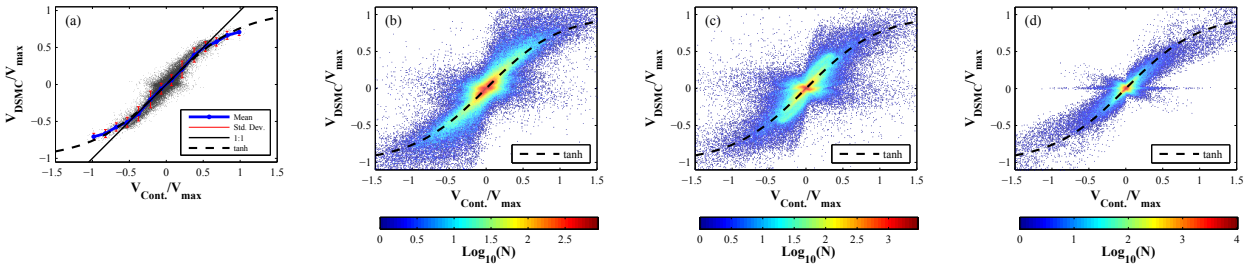

FIGURE 4. Scaled DSMC versus Continuum diffusion velocities for a single case (a) 50:50 He:Ar expansion jet simulation as well as log plots of accumulated point counts for jet simulations from 10% - 90% of each component for (b) He:Ar system, (c) He:Xe system, and (d) Ar:Xe system.

Assuming the *tanh* curve represents a reasonable first approximation, we can estimate the potential error in the continuum diffusion velocity. We expect 2% error around $V_{max}/4$, but this value jumps to 7.5% error when that diffusion velocity doubles. Depending on the other errors in the application and sensitivity of the solution to these errors, this provides insight on the range of applicability. Cases with stronger shocks than those resulting from these expansion jets are needed to populate the higher expected continuum diffusion velocities to ensure that the deviation continues and to verify saturation of the upper bound.

In the future we hope to apply the *tanh* curve as the factor on the thermal velocity limit in a full continuum flow calculation to determine if the change can extend the range of applicability for this model though other continuum breakdowns are likely. We would also like to investigate if this estimated deviation can be used to switch between algorithms in a hybrid Monte-Carlo continuum code and determine how convergence is effected as a function of the expected deviation.

REFERENCES

1. A. L. Garcia, J. B. Bell, W. Y. Crutchfield, and B. J. Alder, *Journal of Computational Physics* **154**, 134 – 155 (1999).
2. J. B. Bell, A. L. Garcia, and S. A. Williams, *ESAIM: M2AN* **44**, 1085–1105 (2010).
3. Z. Dragojlovic, and F. Najmabadi, *Fusion Science and Technology* **47**, 1152–1159 (2005).
4. Z. Dragojlovic, F. Najmabadi, and M. Day, *Journal of Computational Physics* **216**, 37 – 51 (2006).
5. R. Martin, M.S. thesis, University of California, San Diego (2007).
6. F. S. Sherman, *Journal of Fluid Mechanics* **8**, 465–480 (1960).
7. R. E. Center, *Physics of Fluids* **10**, 1777–1784 (1967).
8. G. A. Bird, *Journal of Fluid Mechanics* **31**, 657–668 (1968).
9. R. Kee, G. Dixon-Lewis, J. Warnatz, M. Coltrin, and J. Miller, Sandia National Laboratories Report SAND86-8246, Albuquerque, NM and Livermore, CA (1986).
10. D. Gutkowicz-Krusin, M. A. Collins, and J. Ross, *Physics of Fluids* **22**, 1443–1450 (1979).
11. D. Gutkowicz-Krusin, M. A. Collins, and J. Ross, *Physics of Fluids* **22**, 1451–1460 (1979).
12. J. R. Abernathey, and F. Rosenberger, *Physics of Fluids* **24**, 377–381 (1981).
13. V. Giovangigli, *Multicomponent Flow Modeling*, Birkhäuser, Boston, 1999.
14. R. Herczynski, M. Tarczynski, and Z. Walenta, "Shock Waves in Binary Gas Mixtures," in *Proceedings of 15th International Symposium on Shock Waves and Shock Tubes*, edited by D. Bershader, and R. Hanson, Stanford University Press, Stanford CA, 1986, pp. 713–719.
15. E. Oran, and J. Boris, *Numerical Simulation of Reactive Flow*, Cambridge University Press, Cambridge, UK, 2001.
16. D. E. Rothe, *Physics of Fluids* **9**, 1643–1658 (1966).
17. D. Rothe, University of Toronto Institute for Aerospace Studies Report 114, Toronto, Canada (1966).
18. G. Bird, *Molecular Gas Dynamics and the Direct Simulation of Gas Flows*, Oxford University Press, Oxford, UK, 1994.
19. D. Rothe, personal communication (2010).